2022 International Conference on Manipulation, Automation and Robotics at Small Scales (MARSS) | 978-1-6654-5973-0/22/$31.00 ©2022 IEEE | DOI: 10.1109/MARSS55884.2022.9870485

Automated Fabrication of Tactile Sensors Using a Custom Additive Manufacturing Platform

Danming Wei, *Student Member, IEEE*, Ruoshi Zhang, Ji-Tzuoh Lin, Dilan Ratnayake, Olalekan O. Olowo, Andrew S. Nimon, Moath Alqatamin, Andriy Sherehiy, and Dan O. Popa*

***Abstract*— This paper presents the NeXus, a precision robotic platform with additive manufacturing capabilities that can be used to prototype strain gauge-based tactile sensors – SkinCells - on flexible substrates. An Aerosol Inkjet printer was employed to print the strain gauge structure of the SkinCell sensor. The design of this sensor combines curvilinear geometries representing both a radial shape structure and an arc shape structure, which have opposite gauge responses when the force is applied to the center of the sensor. The fabrication process of the SkinCell sensor is predicated on a parametric kinematic calibration of the NeXus to identify features on the sensor substrate and align them to the printing and metrology tools. Several strain gauge SkinCell sensor samples were printed on pre-fabricated flexible substrates using the NeXus. Results indicate a calibration precision of approximately 170 microns with 60 microns line-width features. This precision is sufficient to ensure that all printed gauges are electrically connected to the pre-fabricated contacts.**

I. Introduction

Additive manufacturing technologies are emerging approaches to creating 3D objects that have already been widely employed in various applications, such as medical implants [1], transportation [2], aerospace [3], energy, and consumer products. In the 1980s, additive manufacturing began to be used for developing prototypes, known as rapid prototyping. Currently, additive manufacturing can be used to create exotic functional products, like robotic skin sensors, smart fabrics, and soft robots.

In the context of additive manufacturing with robots, custom multi-robot platforms have been designed and developed for printing, assembly, and packaging of functional sensors and actuators. M^3 [4-6] was a macro-meso-microscale robotic assembly and packaging platform for Micro-Electro-Mechanical Systems (MEMS) devices. It had a macroscale meter-size workspace with 4 high-precision robots and a vision system for positioning, assembly, and packaging optical fibers with 125 μm diameter. μ^3 [7] was a meso-micro-nanoscale assembly system consisting of 19 degrees of freedom (DOF) with 3 high-precision manipulators as well as additional microgrippers and stereo microscope vision. It was designed to assemble 2½D microparts 50 μm in size that were fabricated on a Silicon wafer. Both M^3 and μ^3 are designed following Lean Robotic Micromanufacturing (LRM) design principles, uniquely applied to manufacture with high yield at a small scale.

In the past several years, Electro-Hydro-Dynamic (EHD) ink-jetting techniques were adopted to print mm-size tactile sensor designs with interdigitated electrodes (IDEs) by 10-micron feature resolution [8]. Later, we developed the fabrication process of the IDE structure of the SkinCell sensor using MEMS fabrication techniques in the cleanroom [9]. To improve the sensitivity and compensate for the temperature drift, we fabricated double-layer sensor arrays with a lamination process [10, 11]. The parametric investigation of the double-layer sensor array is documented in [12]. On the top of the IDEs, a conductive organic piezoresistive material of poly (3,4-ethylene dioxythiophene) polystyrene sulfonate or PEDOT: PSS was applied as the active tactile sensing agent [10, 11]. However, due to the complexity of the cleanroom fabrication process of the SkinCell sensors, the reliability of the sensors and the fabrication yield were not satisfactory.

In this paper, the fabrication process of the SkinCell sensor is realized through additive manufacturing techniques integrated within the NeXus platform. Among other robots, the NeXus features a 6-DOF micropositioner with a micro-resolution, and meter travel range, servicing an Aerosol Inkjet print head, optical microscope, and Intense Pulse Light (IPL) sintering station technique to directly print the sensor structure on the substrate in a more repeatable and reliable manner than the cleanroom fabrication process. In the cleanroom, the samples must be transferred among different instruments manually, which causes more fabrication errors. Also, some steps, such as metal lift-off, have a low manufacturing yield. However, in the NeXus system, the user just loads the substrate on the sample chuck, then monitors the fabrication process remotely until the process is done by the robotic and additive manufacturing systems using precision positioners and microscope vision feedback.

We investigated the kinematic calibration of the NeXus and proposed a parametric least squares identification technique to align the substrate features with the printer nozzle. The precision of the pre-fabricated flexible substrate comes with alignment marks and electrical contact pads, on which the SkinCell strain gauge was printed. The resulting strain gauge features were measured using an optical microscope and compared with their nominal design values. The measured calibration precision of the sensor printing, defined as deviation from Computer Aided Design (CAD) models to the manufactured sensor was smaller than 200 microns. This value was lower than half the size of electrical contact pads, thus ensuring the electrical continuity of the sensor.

This paper is organized as follows: Section II describes the design of the NeXus system and prototype design of a strain gauge SkinCell sensor; in Section III, we present the kinematic design and calibration of the NeXus system for the strain

* Authors are with Louisville Automation and Robotics Research Institute at University of Louisville, Louisville, KY 40208 USA. (e-mail: danming.wei@louisville.edu).

gauge sensor printing; in Section IV, the experimental results are presented and discussed; in Section V, we conclude the paper.

II. NEXUS SYSTEM AND TARGET SENSOR

A. NeXus System

NeXus is a custom multi-scale additive manufacturing robotic system integrated with robotic assembly and 3D printing tools depicted in Fig. 1. It has several subsystems, including industrial robotic arms, a custom 6-DOF positioner, an Aerosol Inkjet printing station, a 3D FDM printing station, a PicoPulse® deposition station, and an intense pulse light (IPL) sintering station. It also includes a microassembly station, an e-textile loom station, and a tool changer with multiple tools for two industrial robotic arm manipulators.

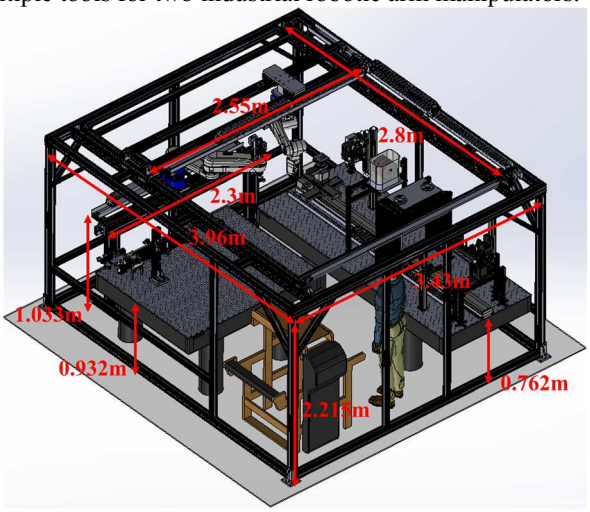

Figure 1. CAD model and dimension of NeXus system, featuring a precision sensor manufacturing line, a precision SCARA robot for electronics, and an overhead dexterous industrial robotic arm for sample transport between the processing stations

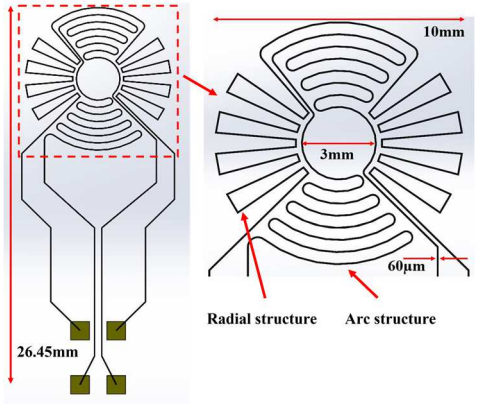

Figure 2. Combined design of strain gauge structure of the tactile sensor, featuring 60 microns width lines arranged in arc and radial shape patterns.

Precision evaluation of the NeXus has been investigated for microsystem integration [13]. Several other helper functions of the NeXus system have been implemented, such as an automated robotic tool change strategy with RGB-D camera assistance [14]. Certain ink materials have been characterized by the Aerosol Inkjet printer in NeXus for strain gauge structures on flexible surfaces [15]. The gauge factor of silver ink deposited by our NeXus system was found to be 1.85 via experiments, which is almost matching mass-produced commercial products.

B. Skin Tactile Sensor Design

In previous work [9-11], we fabricated and laminated double-layer sensor arrays with two same IDE strain gauge structures. The sensors were coating PEDOT: PSS to compensate for temperature drift and enhance force reaction performance. Instead of making the double-layer sensor arrays, a prototype design of a strain gauge structure of the SkinCell sensor, which combines radial and arc structures (shown in Fig. 2), has been designed and printed. The advantage of this combined structure is that it can be printed on only one side of the substrate and when the force is applied to the center of the sensor, the strain gauge performances of the two structures are opposite. The resistance of the radial structure is increasing, while the resistance of the arc structure is decreasing. The SkinCell sensor is one of the demonstrators that can be fabricated on the NeXus system, but other applications are also being pursued, including microrobot assemblies, PCB assemblies, and e-textiles.

C. The Precision Sensor Manufacturing Line of NeXus

Due to the complexity of the cleanroom fabrication process of the SkinCell sensors and the low repeatability and the yield of the product during the fabrication and lamination process, a new strain gauge sensor fabrication process was developed via the NeXus system using OPTOMEC® Aerosol Inkjet printer to print the strain gauge structure of SkinCell tactile sensor on the flexible Kapton® substrate. This method can reduce the fabrication procedures and increase the repeatability and yield of products. In the NeXus, several subsystems were employed to fabricate strain gauge sensors, such as OPTOMEC® Aerosol Inkjet printing station, microassembly station, and the 6-DOF positioner (shown in Fig. 3). Here, an oven was used to cure or sinter the strain gauge structures printed by the Aerosol Inkjet printer. The IPL station will be employed to complete the sintering or curing process in the future.

To carry the substrate, a custom 6-DOF positioner has been designed and assembled in the NeXus as shown in Fig. 4.

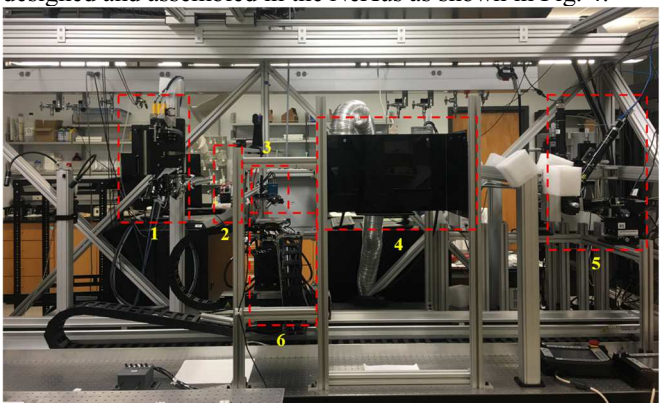

Figure 3. Hardware on a long optical table: 1. OPTOMEC® Aerosol Inkjet printing station; 2. 3D FDM printing station; 3. PicoPulse® inkjet deposition station; 4. Intense Pulse Light (IPL) station; 5. Microassembly station; 6. 6-DOF positioner with the printed sample.

It contains a long linear stage X_L (IAI® ISPB-LXMX-200) and 5 high-precision motorized stages, including two linear stages X and Y (Newport® M-ILS300LM-S), a Z stage

(Newport® GTS70VCC), a tilt stage (Newport® BGS80PP), and a rotation stage (Newport® URS50CPP). They were arranged and assembled from bottom to top in order of X_L-Y-X-Z-T-R. On the top of the rotation stage, an ATI QC-11 tool change coupler was used to mount the sample chuck. The kinematic design of this positioner was discussed in [16] and the measured precision figures of merit are shown in Table I.

TABLE I. PRECISION FIGURES OF MERIT OF 6-DOF POSITIONER

	X_L	Y	X	Z	Tilt	Rotation
Travel (mm)	2500	300	300	70	90 deg	360 deg
Accuracy (µm)	-	2.5	2.5	1.75	30mdeg	25mdeg
Repeatability (µm)	17	5	5	0.5	2.5mdeg	1mdeg
Resolution (µm)	10	0.01	0.01	0.25	0.2mdeg	0.5mdeg

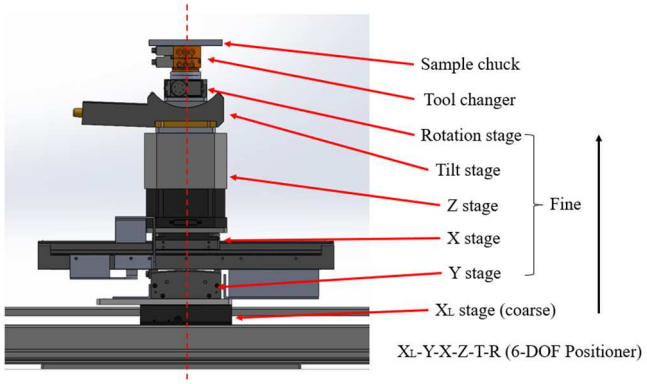

Figure 4. CAD model of the 6-DOF positioner, featuring a coarse X, fine XYZ translation, tilt, and rotation.

III. KINEMATIC DESIGN AND CALIBRATION OF NEXUS

Fig. 5 depicts the coordinate system of each NeXus process station, including additive manufacturing, curing, and metrology tools. For the strain gauge structure printing, it is first necessary to kinematically calibrate the coordinate systems of substrate [S], the 6-DOF positioner [O], OPTOMEC® Aerosol Inkjet printer head [H], and microscope camera [C], and measure the resulting gauge dimension in order to estimate calibration errors. The remaining part of this section discusses three calibration procedures employed to align the printing tool with the sample by means of optical metrology.

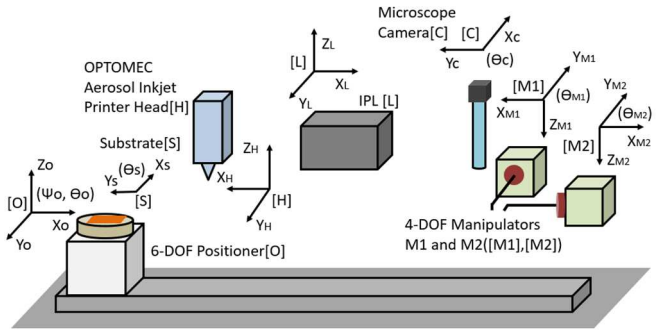

Figure 5. Coordinate frame and distribution of each subsystem for the skin sensor fabrication process in the NeXus.

A. Alignment of the center of sample chuck and printer head

The OPTOMEC® Aerosol Inkjet printer was mounted on the NeXus frame attached to an optical table. The width of the printed line was determined by adjusting several process parameters in its controller, such as sheath flow rate, atomizer flow rate, and atomizer current, as well as the stage motion speed of the 6-DOF positioner. The printing parameters have been characterized in [15, 17]. using a Design of Experiments approach for printing lines with 60-100µm width. After mounting the OPTOMEC printer nozzle, the X-Y-Z coordinates of the printer head are assumed to be constant with respect to the global origin. Before loading the substrate on the sample chuck, a reference point (the center of the sample chuck) was defined on the sample chuck to approximately identify the fiducial coordinates on the substrate when the origin of the substrate matches the center of the sample chuck closely after loading the substrate. In the kinematic calibration process, the center of the field of view (FOV) of the vertical camera in the microassembly station is defined to be the global origin [C] as this camera is fixed on the NeXus frame and the origins of other stations' coordinate systems are considered unknown and will be referred to it.

To align the center of the sample chuck with the OPTOMEC® printer head, we first locate the coordinate of the center of the sample chuck by moving the 6-DOF positioner along with the long linear stage while adjusting other stages to make the center of the sample chuck reach the center of the FOV of the vertical camera in the microassembly station. The current [X_{SC}, Y_{SC}] values of the 6-DOF positioner are the coordinate of the center of the sample chuck with respect to the global origin [C]. For simplicity, the Z height and X_L movements are considered to be fixed during printing and metrology and are not considered in the identification process.

Second, in order to locate the printer head's coordinate, the 6-DOF positioner was moved under the OPTOMEC® station, the Y-X-T-R stages of the 6-DOF positioner were kept at their initial position and only the Z stage was moved up to keep the 4mm distance between the substrate surface and the tip of the Aerosol Inkjet printer head. A cross pattern was printed on a glass slide loaded on the sample chuck, then the 6-DOF positioner moved under the camera and adjusted its position to align the center of the cross to match the center of the FOV of the camera. The current [X_H, Y_H] values of the 6-DOF positioner are the coordinate of the Aerosol Inkjet printer head with respect to the global origin. The offsets [ΔX, ΔY] between the center of the sample chuck and the Aerosol Inkjet printer head were calculated as (Fig. 6):

$$\begin{bmatrix}\Delta X\\ \Delta Y\end{bmatrix} = \begin{bmatrix}X_H\\ Y_H\end{bmatrix} - \begin{bmatrix}X_{SC}\\ Y_{SC}\end{bmatrix} \quad (1)$$

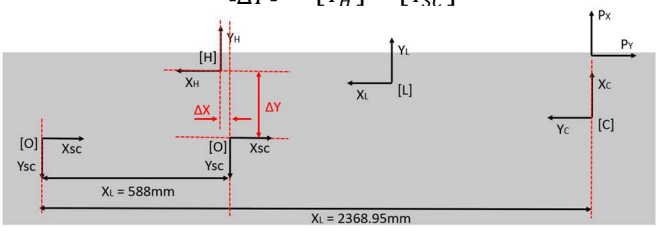

Figure 6. Top view of the alignment of the center of sample chuck to the printer head.

Third, based on the measured offsets between the center of the sample chuck and the Aerosol Inkjet printer head, they can be aligned as shown in Fig. 7. Table II displays the traveling distance of the long linear stage for each station during this

process. When the 6-DOF positioner arrives at each station with the long linear stage, the long linear stage will not move anymore, and only Y-X-Z-T-R stages above it are fine-adjusted to reach the target positions on the sample chuck.

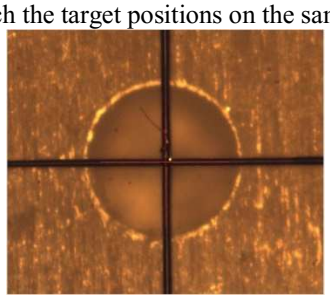

Figure 7. Alignment of sample chuck center and OPTOMEC printer nozzle.

TABLE II. IAI LINEAR STAGE TRAVEL FOR EACH STATION

Location of Station	Linear Stage Travel
Initial Position	0 mm
OPTOMEC® station	588 mm
3D FDM printer station	844.65 mm
PicoPulse® station	1080.65 mm
IPL station	1565.3 mm
Vertical Camera	2368.95 mm

B. *Inverse Kinematic Calibration*

After the alignment of the center of the sample chuck and the printer head, the center of the sample chuck is defined as the reference point for aligning and loading the substrate on the sample chuck. For example, an arbitrary point (X_0, Y_0, θ_0) on the sample chuck with a certain angle θ rotation is desired to be moved to the center of the sample chuck. The mathematical relationship for the inverse kinematic function can be expressed in the following equations (Fig. 8):

$$\theta_0 = \tan^{-1} {}^{Y_0}/_{X_0}, \theta_1 = \theta_0 + \theta \quad (2)$$

$$D = \sqrt{X_0^2 + Y_0^2} \quad (3)$$

$$X_1 = D\cos\theta_1, Y_1 = D\sin\theta_1 \quad (4)$$

where $X_0, Y_0,$ and θ_0 are the initial coordinate of the arbitrary point on the substrate with respect to the center of the sample chuck, θ is the desired orientation, $X_1, Y_1,$ and θ_1 are the calculated coordinate of the new position of the arbitrary point after θ degrees rotation.

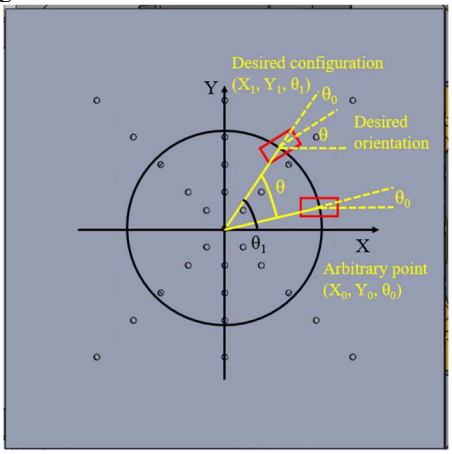

Figure 8. An arbitrary point moves to the center of the sample chuck with the desired orientation.

Here, $X_0, Y_0,$ and θ are inputs, the values of X_0 and Y_0 can be measured from the CAD layout referred to the origin of the substrate. When loading the substrate on the sample chuck, the origin of the substrate needs to be aligned with the center of the sample chuck approximately so that the value of X_0 and Y_0 will be estimated with respect to the center of the sample chuck, while θ_0 and D can be calculated through the values of X_0 and Y_0. X_1 and Y_1 are the calculated outputs, which will determine the relative motions of the X and Y stages to move the arbitrary point to the center of the sample chuck with θ orientation. Last, this arbitrary point can be the starting point for printing structure by the OPTOMEC® Aerosol Inkjet printer. Finally, the calibrated distance [ΔX', ΔY'] between the arbitrary point and the printer head can be calculated by:

$$\begin{bmatrix} X_1 \\ Y_1 \\ \theta \end{bmatrix} = \begin{bmatrix} \cos\theta_1 & 0 & 0 \\ 0 & \sin\theta_1 & 0 \\ 0 & 0 & 1 \end{bmatrix} \begin{bmatrix} D \\ D \\ \theta \end{bmatrix} \quad (5)$$

$$\begin{bmatrix} \Delta X' \\ \Delta Y' \end{bmatrix} = \begin{bmatrix} X_H \\ Y_H \end{bmatrix} - \begin{bmatrix} X_1 \\ Y_1 \end{bmatrix} \quad (6)$$

C. *Visual Servoing Calibration*

When the substrate is loaded on the sample chuck, the origin of the substrate is aligned with the center of the sample chuck. Thus, the coordinates of all features on the substrate can be known with respect to the center of the sample chuck based on the design layout of the substrate. Even though the alignment is as good as possible, there still exist offsets in translation and rotation when a pre-fabricated substrate fiducial mark is brought into the camera's FOV with the inverse kinematic calibration mentioned above. The center of the fiducial mark can be further fine-adjusted to move to the desired orientation and position in the camera's FOV with a visual servoing function. The equations below express the relationship between the difference in the configuration of the center of the template in image pixels and the difference in the stages' movements with the image Jacobian involved. $\Delta P_X, \Delta P_Y,$ and ΔP_θ are the differences in the configuration of the template center in pixels, $\Delta X, \Delta Y,$ and $\Delta\theta$ are the difference in the stages' motion, while the image Jacobian J_{image} is expressed as:

$$\begin{bmatrix} \Delta P_X \\ \Delta P_Y \\ \Delta P_\theta \end{bmatrix} = J_{image} \times \begin{bmatrix} \Delta X \\ \Delta Y \\ \Delta\theta \end{bmatrix} \quad (7)$$

$$J_{image} = \begin{bmatrix} J_{11} & J_{12} & J_{13} \\ J_{21} & J_{22} & J_{23} \\ J_{31} & J_{32} & J_{33} \end{bmatrix} \quad (8)$$

Since the image Jacobian is a 3 x 3 matrix that has 9 entries, a linear least squares estimation method was applied to find the entries' values of the image Jacobian. After the image Jacobian was defined, the center of the template was moved to the desired position and orientation achieved by the following equation:

$$\begin{bmatrix} X_{new} - X_c \\ Y_{new} - Y_c \\ \theta_{new} - \theta_c \end{bmatrix} = \Delta s \times J_{image}^{-1} \begin{bmatrix} P_{X_d} - P_{X_c} \\ P_{Y_d} - P_{Y_c} \\ P_{\theta_d} - P_{\theta_c} \end{bmatrix} \quad (9)$$

where $X_c, Y_c, \theta_c, X_{new}, Y_{new},$ and θ_{new} are the current and new configuration of the 6-DOF positioner; $P_{X_d}, P_{Y_d}, P_{\theta_d}, P_{X_c}, P_{Y_c},$

and P_{θ_c} are values in pixel of the desired and current position and orientation of the center of the fiducial mark in the camera's FOV, Δs represents a step size of the stages' movements. Based on the vision feedback values, the fiducial mark can be moved to the desired position and orientation in a fast and precise method by using the visual servoing technique. After the visual servoing adjustment, the starting point for printing can be located more precisely and matched the tolerance of the printing.

IV. RESULTS AND DISCUSSIONS

A. Experimental Results: Kinematic Calibration

After kinematic calibration of the NeXus for skin tactile sensor fabrication, the designated substrate is loaded on the sample chuck and aligned. By using the inverse kinematic calibration, the fiducial mark was moved into the FOV of the camera and then using visual servoing calibration, the fiducial mark was adjusted to the desired position and orientation with the image Jacobian assistance. The value of the image Jacobian was calculated by the least-squares method by collecting 50 random X, Y, and θ values of the center of the fiducial mark. Fig. 9 depicts the fiducial mark location before and after the visual servoing calibration. The desired position is the center of the camera's FOV, the desired orientation is 0-degree. In the visual servoing calibration, there has a +/- 1 pixel (around 1.33µm) tolerance in translational adjustment and a +/- 0.5-degree tolerance in rotational adjustment.

$$J_{image} = \begin{bmatrix} -0.0003315 & 0.00125767 & 0.281908 \\ -0.0017776 & 0 & 0.302763 \\ 0 & 0 & -1 \end{bmatrix} \quad (10)$$

B. Experimental Results: Printing Precision

After the fiducial mark was aligned to the center of the camera's FOV, the starting point for printing need to be determined on the contact pad. Here, the center of the pad-4 was selected for the starting point for printing and moved to the center of the FOV of the camera by the layout dimension 11.27mm x 31.47mm in Fig. 10. Due to the uncertainties of the calibration process, the printing precision was investigated with 5 samples. The starting point for the printing strain gauge structure was measured on the contact pad-4 compared with the design in the CAD model as shown in Fig. 11, while the endpoint was measured on the contact pad-3. Based on the CAD model, the tolerance for printing a functional gauge is 650µm (half of the 1.3mm pad size), but the actual measured tolerance for printing on the manufactured contact pad is around 620µm. The distances between the center of the fiducial mark to the center of the pad-3 and pad-4 were measured and listed in Table III and the offsets of starting point on the center of the pad-4 and the endpoint on the center of the pad-3 were measured and listed in Table IV.

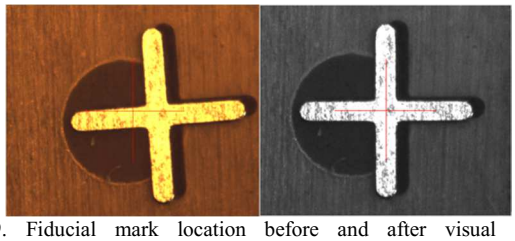

Figure 9. Fiducial mark location before and after visual servoing adjustment.

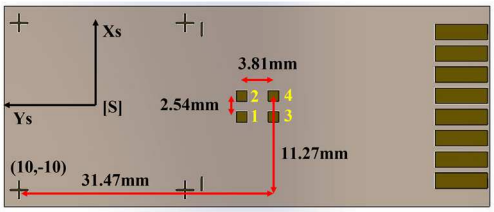

Figure 10. Dimension of fiducial and contact pads on the substrate.

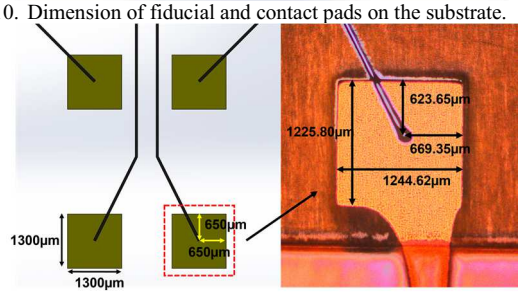

Figure 11. Dimension of the starting point on pad-4 of sample-3.

A calibration precision metric, Cal_P, was defined to express the standard deviation of the difference of the distances between the center of the fiducial mark to the center of the contact pads in layout design and actual manufactured substrate shown in Table III, as well as the offsets of the starting point to pad-4's center and endpoint to pad-3's center compared with the actual locations of the starting point and endpoint printed on pad-4 and pad-3 shown in Table IV. The equation is expressed as below:

$$Cal_P = \sqrt{\sum_{i=1}^{N}[(\Delta X_i + \Delta X_i')^2 + (\Delta Y_i + \Delta Y_i')^2]}/_N \quad (11)$$

where ΔX_i and ΔY_i are the difference in the distance between the center of the fiducial to the center of pad i and in the measured samples and the CAD model layout. $\Delta X_i'$ and $\Delta Y_i'$ are the offsets between the starting point on pad i and the center of the pad, while N is the number of the contact pads considered. The resulting calibration precision using N=2 (pad-3 and pad-4) are listed in Table V. distances between the fiducial to centers of pad-3 and pad-4 in the CAD model and measured samples.

TABLE III. DISTANCES BETWEEN FIDUCIAL TO THE CENTER OF PAD-3 AND PAD-4 IN CAD MODEL AND MEASURED SAMPLES

Sample	Distance between fiducial to the center of the pad-3 and pad-4 (Unit: mm)			
	Pad-3		*Pad-4*	
	X	***Y***	***X***	***Y***
CAD	8.73	31.47	11.27	31.47
Sample-1	8.535	31.516	11.063	31.532
Sample-2	8.532	31.57	11.082	31.6
Sample-3	8.59	31.507	11.132	31.512
Sample-4	8.536	31.525	11.076	31.537
Sample-5	8.53	31.508	11.07	31.53
	ΔX	***ΔY***	***ΔX***	***ΔY***
Sample-1	-0.195	0.0459	-0.207	0.062
Sample-2	-0.198	0.0999	-0.188	0.13
Sample-3	-0.14	0.0369	-0.138	0.0419
Sample-4	-0.1941	0.0549	-0.194	0.0669
Sample-5	-0.2	0.038	-0.2	0.06

The average calibration precision Cal_P=169.1μm ±28.2μm is large, but it is mostly due to manufacturing tolerances of the pre-fabricated substrates, and much less to the robotic precision of the NeXus. Even so, the calibration precision is considerably less than the printing tolerance on the contact pads, which is around 620μm (Fig. 11).

TABLE IV. OFFSETS OF THE STARTING POINTING TO THE CENTER OF PAD-4 AND THE ENDPOINT TO THE CENTER OF PAD-3

Sample	Offsets of the starting point to the center of the pad-4 and the endpoint to the center of the pad-3 (Unit: μm)			
	Pad-3		*Pad-4*	
	ΔX'	*ΔY'*	*ΔX'*	*ΔY'*
Sample-1	-68.5	-35.6	-85.4	-16.1
Sample-2	-56.6	-46.4	-74.6	-63.8
Sample-3	-87.4	-72.6	-81.3	-88.7
Sample-4	-89.4	-82.0	-93.4	-90.1
Sample-5	-109.9	-83.3	-101.2	-102.2

TABLE V. CALIBRATION PRECISION OF THE SENSOR PRINTING

Sample	Calibration precision (μm)
Sample-1	147.5
Sample-2	214.3
Sample-3	132.3
Sample-4	179.5
Sample-5	171.6
Average	169.1
Standard Deviation	28.2

V. CONCLUSION

Instead of fabricating strain gauge skin tactile sensors in the cleanroom using MEMS fabrication techniques, the NeXus system was developed and kinematically calibrated for strain gauge sensors fabrication on the flexible Kapton® substrate. Three calibration procedures were employed to align the printing tool with the samples by means of optical metrology. Inverse kinematic and visual servoing calibration techniques were applied to calibrate the OPTOMEC® Aerosol Inkjet printer nozzle with the starting point for printing the sensor on the substrate more precisely. During the visual servoing calibration process, the precision of calibration results of the fiducial mark is around +/-1.33μm in translation and +/-0.5 degrees in rotation. The calibration precision for the sensor printing is smaller than 200 microns, which is considerably less than the printing tolerance on the contact pads.

ACKNOWLEDGMENT

This work was supported by National Science Foundation awards MRI #1828355 and EPSCOR #1849213. We would like to thank Brian Goulet and Douglas Jackson for their help with the hardware setup and experiments.

REFERENCES

[1]J. Giannatsis and V. Dedoussis, "Additive fabrication technologies applied to medicine and health care: a review," *The International Journal of Advanced Manufacturing Technology,* vol. 40, no. 1, pp. 116-127, 2009.

[2]Y. Song, Y. Yan, R. Zhang, D. Xu, and F. Wang, "Manufacture of the die of an automobile deck part based on rapid prototyping and rapid tooling technology," *Journal of materials processing technology,* vol. 120, no. 1-3, pp. 237-242, 2002.

[3]C. L. Thomas, T. M. Gaffney, S. Kaza, and C. H. Lee, "Rapid prototyping of large scale aerospace structures," in *1996 IEEE Aerospace Applications Conference. Proceedings*, 1996, vol. 4: IEEE, pp. 219-230.

[4]R. Murthy, A. N. Das, D. Popa, and H. Stephanou, "M3: Multiscale, deterministic and reconfigurable macro-micro assembly system for packaging of mems," in *Proceedings 2007 IEEE International Conference on Robotics and Automation*, 2007: IEEE, pp. 668-673.

[5]D. O. Popa, R. Murthy, and A. N. Das, "${\rm M}^{3} $-Deterministic, Multiscale, Multirobot Platform for Microsystems Packaging: Design and Quasi-Static Precision Evaluation," *IEEE Transactions on Automation Science and Engineering,* vol. 6, no. 2, pp. 345-361, 2009.

[6]D. Popa, R. Murthy, M. Mittal, J. Sin, and H. Stephanou, "M3-modular multi-scale assembly system for MEMS packaging," in *2006 IEEE/RSJ International Conference on Intelligent Robots and Systems*, 2006: IEEE, pp. 3712-3717.

[7]A. N. Das, P. Zhang, W. H. Lee, D. Popa, and H. Stephanou, "μ 3: Multiscale, deterministic micro-nano assembly system for construction of on-wafer microrobots," in *Proceedings 2007 IEEE International Conference on Robotics and Automation*, 2007: IEEE, pp. 461-466.

[8]C. Nothnagle, J. R. Baptist, J. Sanford, W. H. Lee, D. O. Popa, and M. B. Wijesundara, "EHD printing of PEDOT: PSS inks for fabricating pressure and strain sensor arrays on flexible substrates," in *Next-Generation Robotics II; and Machine Intelligence and Bio-inspired Computation: Theory and Applications IX*, 2015, vol. 9494: International Society for Optics and Photonics, p. 949403.

[9]J. Baptist, R. Zhang, D. Wei, M. Saadatzi, and D. Popa, "Fabrication of strain gauge sensor arrays for tactile skins," in *Proc. SPIE*, 2017, vol. 10216, p. 1021619.

[10] D. Wei, R. Zhang, M. N. Saadatzi, O. O. Olowo, and D. O. Popa, "Organic Piezoresistive Pressure Sensitive Robotic Skin for Physical Human-Robot Interaction," in *International Design Engineering Technical Conferences and Computers and Information in Engineering Conference*, 2020, vol. 83907: American Society of Mechanical Engineers, p. V001T01A013.

[11] O. O. Olowo, R. Zhang, Z. Yang, B. Goulet, and D. O. Popa, "Organic Piezoresistive Robotic Skin Sensor Fabrication, Integration and Characterization," in *International Manufacturing Science and Engineering Conference*, 2021, vol. 85079: American Society of Mechanical Engineers, p. V002T08A013.

[12] M. N. Saadatzi, Z. Yang, J. R. Baptist, R. R. Sahasrabuddhe, I. B. Wijayasinghe, and D. O. Popa, "Parametric investigation of scalable tactile sensors," in *Smart Biomedical and Physiological Sensor Technology XIV*, 2017, vol. 10216: SPIE, pp. 51-60.

[13] D. Wei *et al.*, "Precision Evaluation of NeXus, a Custom Multi-Robot System for Microsystem Integration," in *International Manufacturing Science and Engineering Conference*, 2021, vol. 85079: American Society of Mechanical Engineers, p. V002T07A008.

[14] D. Wei, C. M. Trombley, A. Sherehiy, and D. O. Popa, "Precise and Effective Robotic Tool Change Strategy Using Visual Servoing With RGB-D Camera," in *International Design Engineering Technical Conferences and Computers and Information in Engineering Conference*, 2021, vol. 85451: American Society of Mechanical Engineers, p. V08BT08A028.

[15] D. Ratnayake, A. Curry, and K. Walsh, "Demonstrating a new ink material for aerosol printing conductive traces and custom strain gauges on flexible surfaces," in *2021 IEEE International Conference on Flexible and Printable Sensors and Systems (FLEPS)*, 2021: IEEE, pp. 1-4.

[16] M. H. Saadatzi and D. O. Popa, "Kinematic Analysis of a 5-DOF Positioner for Precision Additive Manufacturing," in *International Design Engineering Technical Conferences and Computers and Information in Engineering Conference*, 2020, vol. 83990: American Society of Mechanical Engineers, p. V010T10A096.

[17] D. Ratnayake, A. T. Curry, C. Qu, J. Usher, and K. Walsh, "Characterizing the Conductivity of Aerosol Jet Printed Silver Features on Glass," in *International Manufacturing Science and Engineering Conference*, 2021, vol. 85079: American Society of Mechanical Engineers, p. V002T08A007.